Tome Gegovski
MSc, assistant
Ss. Cyril and Methodius University in Skopje
Faculty of Civil Engineering
gegovski@gf.ukim.edu.mk

Zlatko Bogdanovski
PhD, Associate professor
Ss. Cyril and Methodius University in Skopje
Faculty of Civil Engineering
bogdanovski@gf.ukim.edu.mk

PSINSAR-BASED DEFORMATION ANALYSIS IN THE SKOPJE AREA

PSInSAR is a multi-interferogram InSAR technique used to determine small displacements in urban environments, utilizing satellite SAR images.

This paper presents the fundamental characteristics of the PSInSAR technique and its application for determining displacements in the Skopje region using 101 Sentinel-1 images.

Keywords: PSInSAR, Skopje area, Sentinel-1, deformation, geodynamics.

1. INTRODUCTION

The monitoring of Earth's crust deformations, resulting from constant seismic processes impacting its surface, is a crucial and increasingly popular field within geodesy, known as geodynamics. Geodynamics has emerged as a distinct discipline focusing on the dynamic changes in the Earth's crust and mantle. The application of traditional geodetic methods for this purpose is often limited, as these methods are not always suited for detailed and frequent monitoring over large areas.

Advances in satellite technology have opened up new possibilities for overcoming previous limitations in monitoring Earth's crust deformations. One well-known geodetic approach for this is GNSS. However, in recent years, SAR (Synthetic Aperture Radar) has gained prominence as a modern technology in remote sensing. SAR captures images that can be used to assess deformations through SAR Interferometry (InSAR), a radar-based technique. InSAR techniques rely on identifying phase differences, or the interferometric phase, in pixels from two SAR images taken at different times to measure surface deformation.

The interferometric phase consists of multiple components, among which the deformation and topographic components are the most important for modeling. However, these are often masked by phase influences caused by atmospheric effects and various signal noises. The topographic component can be modeled using a Digital Elevation Model (DEM), a technique known as Differential InSAR (DInSAR). However, to monitor subtle 'silent displacements' of seismic origin, other components must also be considered, complicating the process further.

One of the most well-known InSAR techniques, which addresses the additional components of the interferometric phase and offers the highest accuracy in measuring Earth's crust deformations, is PSInSAR (Permanent Scatterer InSAR). This paper presents the fundamental characteristics of the PSInSAR approach, supported by a real analysis of the Skopje basin using 101 Sentinel-1 SAR images from 2016 to 2024.

2. ADVANCED MULTI-INTERFEROGRAM TECHNIQUE PSINSAR

2.1. FUNDAMENTAL INSAR CONCEPT

The interferometric phase consists of several components, as expressed in relation (1):

$$\Delta\varphi = \Delta\varphi_{flat} + \Delta\varphi_{elev.} + \Delta\varphi_{disp.} + \Delta\varphi_{atm.} + \Delta\varphi_{n.} \quad (1)$$

The first component, $\Delta\varphi_{flat}$, is not a significant issue for modern SAR satellites, as it can be relatively easily modeled and removed from the interferometric phase. The elevation component, $\Delta\varphi_{elev.}$, is generally corrected using a DEM, however, errors in the DEM or the limited sensitivity of SAR images to this component can still affect the interferometric phase, leading to potential inaccuracies.[2] [10]

The deformation component, $\Delta\varphi_{disp.}$, is the primary focus of this research. However, various atmospheric conditions during the acquisition of SAR images ($\Delta\varphi_{atm.}$), as well as noise ($\Delta\varphi_{n}$) in the images leading to decorrelation, have a significant impact on the interferometric phase. [10]

2.2. THE NEED FOR MULTI-INTERFEROGRAM TECHNIQUE

In [4], we presented the fundamental characteristics of SAR interferometry, which is a relatively new acquisition method. Due to its unique features, it stands out as the only method capable of accurately determining deformations over large areas.

SAR interferometry is a very promising technology, however, it is affected by a series of important problems. Firstly, interferograms are prone to decorrelation, either temporal or geometrical. Secondly, the interferometric phase is wrapped, making it difficult to unwrap accurately using a single interferogram. Additionally, if the topography of the area of interest is not known with sufficient precision, distinguishing between residual topography and actual terrain displacement becomes a challenging task. Finally, even when these issues are addressed, atmospheric artifacts can severely bias the detected signals, undermining the overall analysis. [7]

These challenges highlight the need for advanced approaches, such as multi-Interferogram InSAR techniques like PSInSAR, which provide a robust framework to overcome these limitations and enhance the accuracy of deformation measurements.

2.2. PERMANENT SCATTERER INSAR

The Permanent Scatterer InSAR technique is based on the assumption that atmospheric effects on phase values are spatially correlated in each acquisition, while the deformation component is temporally correlated. This allows for the estimation and removal of the Atmospheric Phase Screen (APS) from each SAR acquisition, thanks to the network of PS points. [9]

The technique consists of the following steps:

1. Creation of differential interferograms;
2. Selection of PS candidates;
3. Spatial-temporal modeling;
4. Phase demodulation and network adjustment of PS points.

2.2.1 Creation of differential interferograms

Since this is a multi-interferogram technique, the first step is to create N interferograms from N+1 SAR acquisitions.

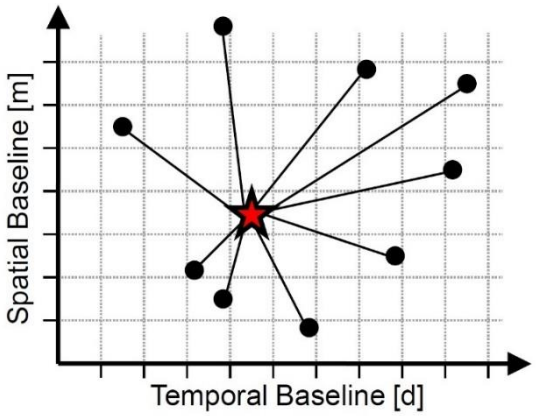

Figure 1. Schematic representation of interferogram generation in PSInSAR. [1]

All interferograms are generated using the same reference image. The choice of the reference image is determined by the need to create interferograms with the smallest possible spatial and temporal baselines. (Figure 1)

The spatial baselines refer to the normal baseline distance between the satellite positions during the two acquisitions. The temporal baseline refers to the time interval between the two acquisitions. In each interferogram, the topographic component is modeled and removed using a digital elevation model (DEM). This type of interferogram is called a **differential interferogram**, and the technique is known as **DInSAR**.

2.2.2 Selection of PS candidates

A Permanent Scatterer (PS) point refers to a scatterer within the resolution cell whose scattering vector has the highest intensity. This results in the resolution cell having a high Signal-to-Noise Ratio (SNR) and a stable phase value over time. As shown in Figure 2, one of the scatterers exhibits a high amplitude value, which is attributed to a high level of reflection.

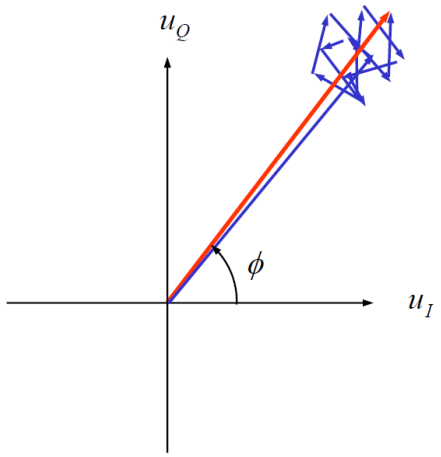

Figure 2. Representation of a Permanent Scatterer within the resolution cell [5]

High amplitude values are observed in scatterers within the resolution cell where dihedral scattering occurs. In this case, almost all the energy reaching that resolution cell is reflected back toward the sensor (Figure3A).

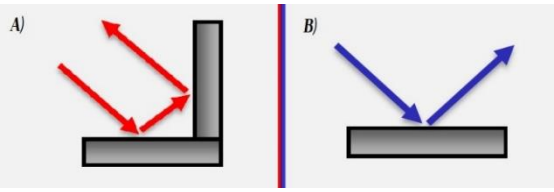

Figure 3. A) Dihedral Scattering B) Specular Scattering

Dihedral scattering most commonly occurs in urban areas, as this type of scattering is characteristic of objects such as buildings. Therefore, PS points are predominantly found in urban environments. However, it can also occasionally occur in rocky terrains.

A very important characteristic of PS points is that they have a stable phase over time, which is not the case with other pixels, such as **DS (Distributed Scatterers).** (Figure 4)

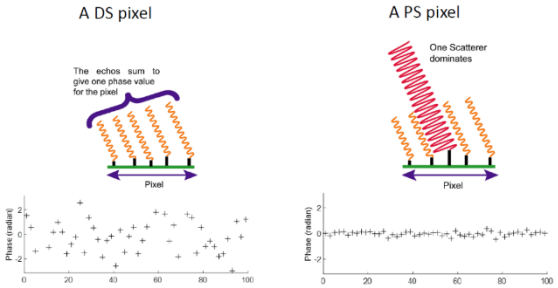

Figure 4. Representation of phase variation in PS and DS pixels. [5]

In the PSInSAR algorithm, a simple solution is proposed for detecting PS points in all N interferograms, based on the determination of the **Amplitude Dispersion Index (DAI)**, which is calculated according to relation (2).

$$D_A = 1 - \frac{\sigma_A}{\mu_A} \qquad (2)$$

Where:

σ_A – The standard deviation of the amplitude of pixel P across all N interferograms.
μ_A– The mean amplitude of pixel P across all N interferograms.

The Amplitude Dispersion Index is calculated for each pixel across all N interferograms. In this process, all SAR images, specifically the layer of the image containing all amplitude values, must be radiometrically calibrated. The selection of PS candidates refers to those pixels with an Amplitude Dispersion Index greater than 0.4 (when using the STaMPS algorithm). To obtain reliable values, at least 30 SAR images are required.

2.2.3 Spatial-temporal modeling

The selection of PS points refers to the process of choosing pixels where the interferometric phase in all created differential interferograms is significantly freed from the systematic influence of phase decorrelation (n), which is reduced to random error ($\Delta\varphi_n$).

On the other hand, the topographic component ($\Delta\varphi_{elev.}$) has already been modeled and largely removed in the creation of differential interferograms. However, errors in elevation must still be considered, and this component will be further treated as a systematic influence, which will depend on the size of the interferogram's baseline. As for the deformation

component it is important to note that its determination is only possible if it is assumed that the displacement is **linear over time**. This assumption limits the application of this technique to areas where deformations follow a linear trend over time. In general, the total deformation is decomposed into two components: linear and nonlinear deformation, where the assumption is that the nonlinear deformation has minimal impact on the overall interferometric phase.

According to the above, the interferometric phase in the i-th interferogram for each PS point is determined according to relation (3):

$$\varphi_i = W\left\{\underbrace{\frac{4\pi}{\lambda}\cdot v\cdot \Delta t}_{\varphi_{def}} + \underbrace{\frac{4\pi}{\lambda}\cdot\frac{B_n}{R\cdot\sin(\theta)}h_{err}}_{\varphi_{topo}} + d_{NL} + \alpha + n_{res}\right\} \quad (3)$$

Where:

W – Modulated interferometric phase with a 2π modulus (Wrapping operator).

$\frac{4\pi}{\lambda}$ – Wavelength conversion factor (λ) into a 2π modulus, multiplied by 2 due to the round-trip signal path from the sensor to the Earth's surface and back.

v – Speed of displacement of the deformation vector (usually expressed in mm/year).

Δt– Temporal baseline of the i-th interferogram.

B_n–Normal baseline distance between the satellite positions in the two acquisitions. For modern satellites, it is calculated with very high accuracy. (Figure 1)

h_{err}–Mean elevation error of the PS (taken from the DEM).

R – Distance from the sensor to the Earth's surface.

θ – Acquisition angle.

d_{NL}–Component related to nonlinear deformation.

α–Component related to non-identical atmospheric effects in the two acquisitions.

n_{res}–Component related to residual phase decorrelation. It is typically a small, insignificant value after selecting the PS points.

According to one of the assumptions of the PSInSAR technique, which involves the spatial correlation of atmospheric influences, this means that the atmospheric components of the interferometric phases at two neighboring PS points will have identical or very similar values. Their difference will be largely free from atmospheric effects. Moreover, this difference will reflect the relative speed of the linear deformation component and the relative elevation errors at the two points. Therefore, the difference in the interferometric phases between neighboring PS points A and B in the i-th interferogram is expressed according to relation (4):

$$\Delta\varphi_{i}{}_{A}^{B} = W\left\{\left[\underbrace{\frac{4\pi}{\lambda}\cdot\Delta t\cdot\Delta\boldsymbol{v}_{\boldsymbol{A}}^{\boldsymbol{B}}}_{\varphi_{def}} + \underbrace{C\cdot B_n\cdot\Delta\boldsymbol{h}_{\boldsymbol{err}}{}_{\boldsymbol{A}}^{\boldsymbol{B}}}_{\varphi_{topo}}\right] + \underbrace{\Delta d_{NL}+\Delta\alpha+\Delta n_{res}}_{phase\ residual\ (\Delta w)}\right\} \quad (4)$$

Where:

Δv_A^B – Relative displacement speed between the two PS points.

C – A constant value for each interferogram, which refers to the product $\frac{4\pi}{\lambda\cdot R\cdot\sin(\theta)}$.

$\Delta h_{err}{}_{A}^{B}$ – Relative mean elevation error between the PS pair.

Δd_{NL} – Value of the nonlinear deformation component.

$\Delta\alpha$ – Difference in atmospheric components between two neighboring PS. If the distance between the PS points is <1 km, it is estimated that $\Delta\alpha$ < 0.1 RAD.

The determination of the spatially dependent component of atmospheric influence is determined by at least 3 to 4 PS points within 1 km². Failure to meet this condition is an additional limiting factor for applying the PSInSAR technique in non-urban areas, where vegetated surfaces predominate. In urban environments, typically, the number of PS points exceeds 50 within 1 km². [3]

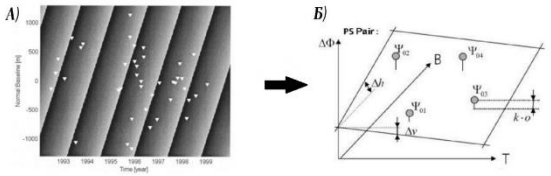

Figure 5. A) Periodogram showing the spatial-temporal dependence; B) Best-fitting 2D plane, whose slopes represent the linear values of the PS pair. [3]

It should be emphasized that the difference in interferometric phase between two points ($\Delta\varphi_{i}{}_{A}^{B}$) still has a modulated phase value within 2π. According to relation (4), the problem is reduced to an equation with two dependent unknowns between the two neighboring PS points, namely:

- Relative speed of the linear deformation component (Δv_A^B), which depends on the temporal baseline Δt;

- Relative elevation error ($\Delta {h_{err}}_A^B$), which depends on the normal baseline distance (Bn).

Assuming that the values for Δv_A^B and $\Delta {h_{err}}_A^B$ are known, the phase residual (Δw) in relation (4) must satisfy the condition (Δw < 0.6).

After determining the values for Δv_A^B and $\Delta {h_{err}}_A^B$, these values are substituted into relation (4), and the phase residual (Δw) is obtained. Based on this, the **temporal coherence (γ)** is calculated, which must be higher than the minimum allowed value (γ_0 = 0.9), satisfying the condition ($\gamma > \gamma_0$). The multi-interferogram coherence ranges from 0 to 1 and is calculated according to relation (5):

$$\gamma = \left| \frac{\sum_{i=1}^{N} e^{j\Delta w}}{N} \right| \quad (5)$$

All PS pairs that, after determining the relative deformation velocities and relative elevation errors, do not satisfy the condition ($\gamma > \gamma_0$) will not proceed to the next step. However, those pairs that meet the condition will participate in the next integration step with a γ-weight.

2.2.4 Phase demodulation and network adjustment of PS points

After determining the values of Δv and Δh_{err} for each pair in the PS point network, these values need to be phase unwrapped according to one of the phase unwrapping algorithms. The most commonly used phase unwrapping algorithm is the SNAPHU algorithm.

Once the unwrapped values of Δv and Δh_{err} for each PS pair are determined, they need to be integrated to obtain absolute values. The process of obtaining the absolute values of the deformation velocity and elevation error for each PS point is done using one of the geodetic network adjustment methods with a datum at a single point (the reference PS point). The most commonly used method is the indirect adjustment using the least squares method.

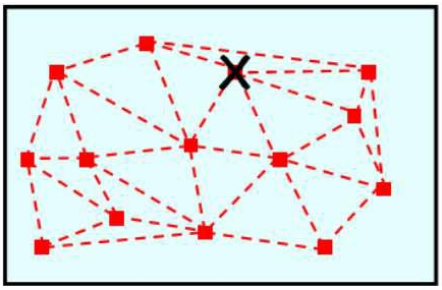

Figure 6. PS network integration [6]

Two separate adjustments are made: one to determine the deformation velocity of the PS points and another to determine the mean elevation errors of the PS points. In the indirect adjustment, the number of measurements equals the number of PS pairs, which represent relative deformation velocity or relative elevation error measurements.

3. PSINSAR FOR THE SKOPJE AREA

3.1. ACQUISITION OF SAR IMAGES

The first step in conducting a PSInSAR analysis is obtaining SAR images. Sentinel-1 images, which are part of the Copernicus program of the European Space Agency (ESA), provide global coverage and are freely available, making them ideal for large-area analysis and long-term deformation monitoring. Users can easily access these data through platforms such as ASF DAAC Vertex or Copernicus Open Access Hub, where the images can be downloaded in various formats.

Given the circumstances, the choice was limited to using exclusively Sentinel-1 SAR images. For this purpose, a total of 101 images were downloaded from the ASF DAAC Vertex platform for the territory of Skopje, from a descending orbit, covering the period from November 11, 2015, to March 16, 2024.

Additionally, the following parameters were used when selecting the images.

Table 1. Parameters used for obtaining SAR images

Orbit type	*Descending*
SAR image type	*L1 SLC*
Beam mode	*IW*
Polarization	*VV*
Orbital path number	80
Frame number	453

4.2. SELECTION OF THE REFERENCE IMAGE AND CREATION OF DIFFERENTIAL INTERFEROGRAMS

In the PSInSAR analysis process, the selection of the reference image plays a crucial role in the accuracy of the final results. For the purposes of this analysis, the image from October 27, 2019, was selected based on several criteria, such as the stability of atmospheric conditions and the quality of the image. Additionally, when selecting the reference image, careful consideration was given to the effects of the

temporal and normal baseline vectors between the reference and secondary images. (Figure 7)

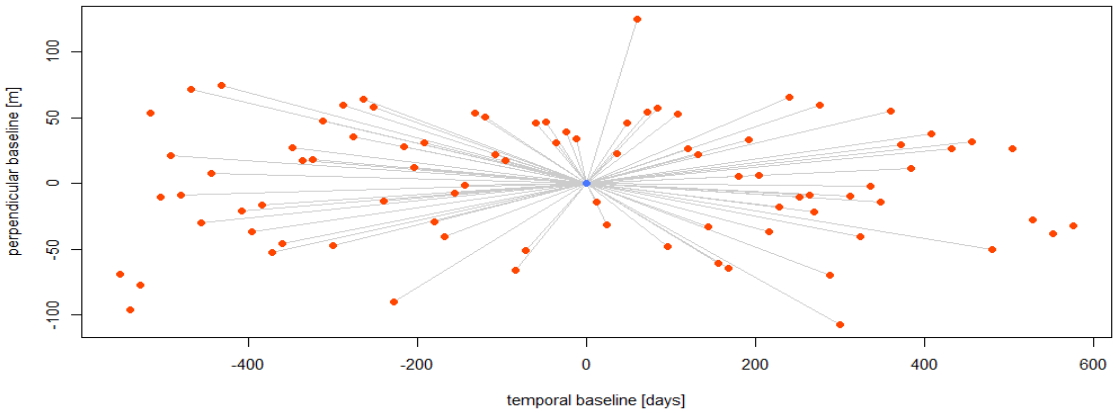

Figure 7. PSInSAR graph of the connection between the reference and secondary images.

It is primarily important to note that for the PSInSAR analysis, the **STaMPS** (Stanford Method for Persistent Scatterers) algorithm, developed by Stanford University, was used. This algorithm is specialized for identifying and analyzing PS points. However, for the creation of differential interferograms, the SNAP (Sentinel Application Platform) software was used, which allows for SAR image processing and data preparation for further analysis with STaMPS.

The process of creating differential interferograms begins with loading the reference and secondary SAR images into the SNAP software, from which a total of 100 differential interferograms will be generated. The first step in the processing is preprocessing, which involves selecting one of the three sub-swaths of the Sentinel-1 images, as well as selecting a precise orbit for the acquisition of the images. The choice of sub-swath is significant as it facilitates processing, since the processing will not be performed on the entire image.

The next step is geocoding each image, where the images are transformed from pixel coordinates to geographic coordinates, enabling their accurate spatial alignment. Radiometric corrections are then applied to improve the spectral characteristics of the images, which is important for further analysis and for reducing noise and some atmospheric effects.

After geocoding and enhancing the spectral characteristics, differential interferograms are generated by comparing each secondary image with the reference image. This enables the calculation of phase differences, which are used to detect deformations. Additionally, reflectivity maps are created for the amplitude values of each secondary image. These maps are utilized to calculate the amplitude dispersion index, which aids in selecting stable ground points (Persistent Scatterers - PS) for analysis.

Since Sentinel-1 images are captured across multiple sub-swaths and bursts, a debursting process is required to synthesize all the strips from each sub-swath into a single continuous image. Furthermore, it is possible to select specific strips to further simplify processing.

The aforementioned process is computationally and time-intensive, as it needs to be performed for all 100 differential interferograms. To streamline and automate the workflow, Python scripts from the *snap2stamps* package were employed. This enabled the automatic generation and processing of differential interferograms. As a result, the entire process was consolidated into two graphs, significantly simplifying the generation of differential interferograms.

It is important to emphasize that the differential interferograms were not created for the entire area of the SAR images, but rather for the region defined by the following WGS 84 ellipsoidal coordinates, listed in Table 2.

Table 2. WGS84 Coordinates of the Area of Interest Subject to PSInSAR Analysis

Longitude minimum	*21° 19’ 15”*
Latitude minimum	*41° 56’ 05”*
Longitude maximum	*21° 39’ 10”*
Latitude maximum	*42° 03’ 35”*

4.3. PSINSAR USING THE STAMPS ALGORITHM

We have already defined that the PSInSAR technique consists of four steps. Through the previous activities in the SNAP software, we generated the differential interferograms, where the interferometric phase includes the components from relation (3).

The PS approach begins by utilizing only those pixels with a high coefficient of the Amplitude Dispersion Index (ADI), defined by relation (2). Since this ADI ranges from 0 to 1, high coefficients are considered to be values above 0.7, indicating a high likelihood of stable phase values. However, this approach may exclude many other pixels with stable phase values but lower ADI coefficients. Therefore, when using the STaMPS algorithm, it is recommended that PS candidates have an ADI of at least 0.4.

The STaMPS algorithm begins precisely with this activity: defining PS candidates, where the $\Delta\varphi_{noise}$ component is either eliminated or has an insignificant influence in relation (3). This is achieved using the *mt_prep_snap* command in a Linux environment. With this command, the algorithm calculates the ADI coefficient for each pixel in the defined area and retains only those pixels with a value above 0.4, referred to as PS candidates.

The STaMPS algorithm is MATLAB-oriented and consists of eight steps:

1. Loading PS candidates: Initial processing of identified PS candidates.
2. Temporal coherence calculation: Calculating the temporal coherence for each PS candidate.
3. PS point selection: Final selection of PS points based on coherence and stability.
4. PS point filtering (PS weeding): Removing redundant or low-quality PS points.
5. Phase correction: Addressing potential phase inconsistencies.
6. Phase unwrapping: Resolving phase ambiguities for the selected PS points.
7. Determination of spatially correlated error components: Correcting errors related to the acquisition angle.
8. Atmospheric filtering of secondary images: Mitigating atmospheric effects across the processed images. [8]

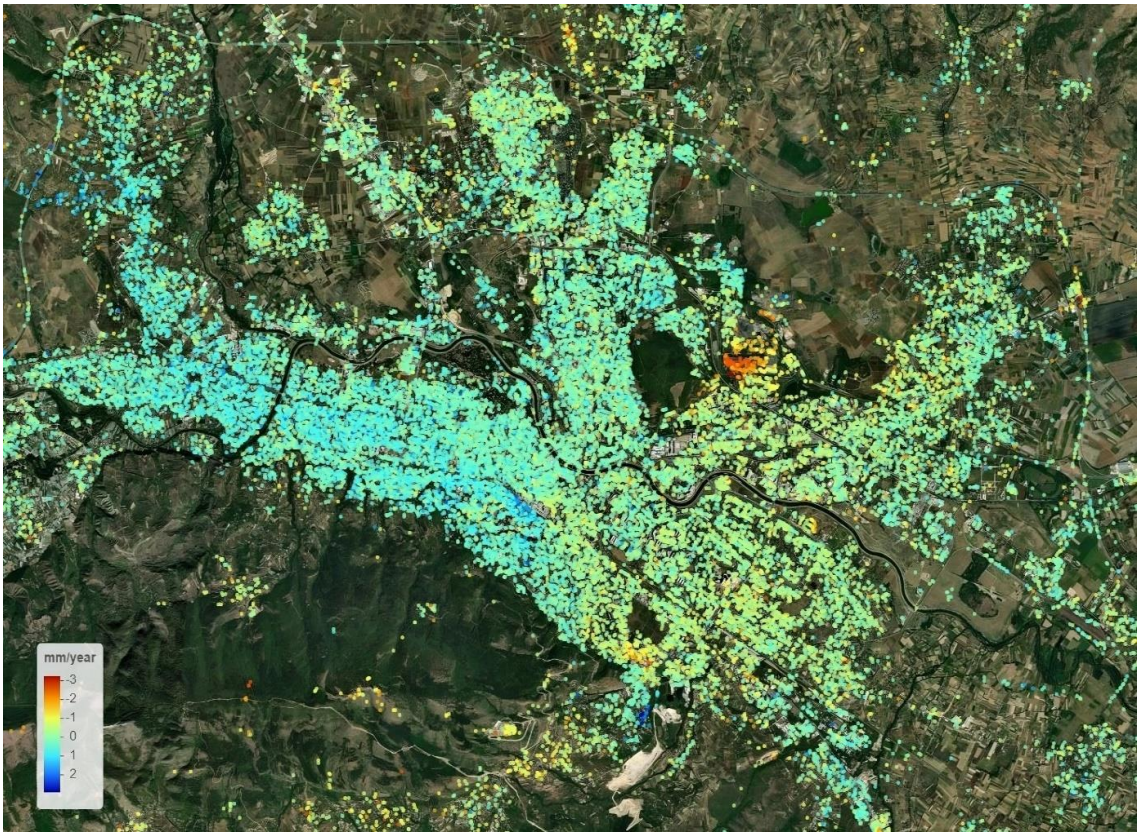

Figure 8. Deformation Results from the Conducted PSInSAR Analysis for the Skopje Basin Displayed in the STaMPS Visualizer Software

After processing all the aforementioned stepsthe $\Delta\varphi_{disp}$ was isolated from the other components in the interferometric phase across all **26 384 PS points**. It is important to note that only linear displacements over time are determined, modeled by the following equation:

$$\Delta\varphi_{disp} = \frac{4\pi}{\lambda}\Delta v B_T \quad (6)$$

From equation (6), it can be observed that the linear deformations are determined as the displacement velocity (*Δv*) in millimeters per year in the acquisition direction.

From Figure 8, the displacements in the Line of Sight (LOS) direction are clearly shown, which in essence slightly differ from the vertical displacements. The results of the PSInSAR analysis indicate that the PS points are mainly positioned in the urban area of the city, as the objects exhibit the characteristics of permanent scatterers (PS). According to Figure 8, in the western part of the Skopje basin, PS points with light blue color dominate, indicating an uplift of 1mm/year, while in the eastern part of the Skopje basin, PS points with a yellowish color prevail, indicating a subsidence of 1mm/year.

4. CONCLUSION

This paper briefly presents the fundamental characteristics of InSAR, with an emphasis on PSInSAR, as the most accurate InSAR technique for determining surface deformations. All of this is supported by a PSInSAR analysis for the territory of Skopje. The results of the PSInSAR analysis clearly show that there is a slight relative displacement between the western and eastern parts of the city, in opposite directions. The western part is moving towards the satellite, indicating a slow uplift of the surface with an average velocity of approximately 1mm/year for the PS points, while the eastern part is moving in the opposite direction, indicating slow subsidence of the surface with an average velocity of around 1mm/year for the PS points. These results provide additional motivation to continue research in the field of InSAR, using additional SAR images, applying different PSInSAR algorithms, and certainly adopting a multidisciplinary approach to interpret the causes of such displacements.

Additionally, further investigation into the long-term trends and potential correlations with other geophysical data could lead to a more comprehensive understanding of the underlying factors contributing to these surface deformations, such as geological activity, urban expansion, or human-induced changes.

5. REFERENCES

[1] ASF. (2023). Radar Community ASF. Retrieved from GEOS 657 Microwave Remote Sensing: https://radar.community.uaf.edu/

[2] EO59. (2024). Advance InSAR training course supported by SARPROZ PSInSAR algorithm.

[3] Ferretti, A., & Rocca, F. (2000). Analysis of Permanent Scatterers in SAR interferometry. IEEE Transactions on Geoscience and Remote Sensing.

[4] Gegovski, T., Bogdanovski, Z., & Kasapovski, F. (2022). A REVIEW OF INSAR TECHNOLOGY FOR DETERMINATION OF SURFACE DEFORMATION. SJCE, 13-19.

[5] Hooper, A. J. (2006). PERSISTENT SCATTERER RADAR INTERFEROMETRY FOR CRUSTAL DEFORMATION STUDIES AND MODELING OF VOLCANIC DEFORMATION.

[6] Minh, D. H. (2021). InSAR course supported by IGARSS.

[7] Perissin, D. (2014). Interferometric SAR MultiTemporal processing (techniques and applications).

[8] RUS Copernicus. (2022). StaMPS: Persistent Scatterer Interferometry Processing. ESA.

[9] UAF University of Alaska Fairbanks. (2024). GEOS F639 901 202401 (CRN 35703) InSAR and Its Applications. Retrieved from https://canvas.alaska.edu/courses/18500

[10] Woodhouse, I. H. (2006). Introduction to Microwave Remote Sensing. CRC Press.